Chapter – 4

Measurement of (n, γ), (n, p) and (n, 2n) reaction cross sections of W and Gd isotopes

---

Publication related to this chapter:

Rajnikant Makwana, S. Mukherjee, P. Mishra, H. Naik, N.L. Singh, M. Mehta, K. Karel, S. V. Suryanarayana, V. Vansola, Y. Shanthisheela, M. Karkera, R. Acharya, S. Khirwadkar, "Measurements of cross sections of ^{186}W (n,γ) ^{187}W, ^{182}W (n, p) ^{182}Ta, ^{154}Gd (n, 2n) ^{153}Gd, ^{160}Gd (n, 2n) ^{159}Gd reactions between 5 to 17 MeV neutron energies"

Physical Review C (Accepted 8th July 2017; In press)

Impact Factor: 3.82

4.1. Introduction

Nuclear reaction cross section data is of prime importance for the reactor technology. When the reactor is in operation, it produces neutrons that penetrate through several materials, such as fuel, structural, controlling and shielding materials, etc. It is important to have nuclear reaction cross section data for all these materials, at all possible neutron energies [1] for the development of the reactor technology. There are numerous measured nuclear data available in the EXFOR data library [2]. However, it is important to have more experimental nuclear data, measured with high accuracy in the energy range between thermal to 20 MeV for a number of reactor materials [2]. Tungsten (W) and gadolinium (Gd) are two such materials. W is selected as a diverter material for the upcoming fusion device – International Thermonuclear Experimental Reactor (ITER) [3]. In ITER the DT reaction generates 14.6 MeV neutrons, which are scattered from the surrounding materials, thus neutrons will have energies from thermal to 14.6 MeV [4-9]. These neutrons interact with the diverter material of the reactor and can open different nuclear reaction channels. In Accelerator Driven Subcritical system (ADSs), W is used in different parts, hence it can face neutrons with higher energies [10]. Further, Gd is an important rareearth element, which is used in control rods. Its nitrate form is useful for reactor control through moderator as liquid poison, as well as a secondary shutdown device in PHWR reactors [11]. Gadolinium nitrate is more advantageous due to its properties, such as; high thermal neutron capture cross section, quick burnout, greater solubility and a more efficient removal by ion exchange systems compared with boron [12]. Hence it is important to have accurate cross section data for all the tungsten and gadolinium isotopes in the energy range from thermal to 20 MeV. Accurate experimental data is also needed to validate the various theoretical nuclear models [13]. In view of this, in the present work, cross sections for the $^{186}W(n, \gamma)^{187}W$, $^{183}W(n, p)^{183}Ta$, $^{154}Gd(n, 2n)^{153}Gd$ and $^{160}Gd(n, 2n)^{159}Gd$ reactions at the neutron energies of 5.08 ± 0.165, 8.96 ± 0.77, 12.47 ± 0.825 and 16.63 ± 0.95 MeV were measured by neutron activation analysis (NAA) and the off-line gamma ray spectrometry technique. The above mentioned reaction cross-sections were also calculated by using the computer codes TALYS – 1.8 and EMPIRE – 3.2.2. Different ldmodels available in TALYS – 1.8 and levden models in EMPIRE – 3.2.2 were used to validate the present experimental results.

4.2. Experimental details

4.2.1 Target Preparation

To conduct the experiment, four samples of W and two samples of GdO_2 were required for the irradiation. The W samples (99.9 % pure) were prepared at the Divertor Group, Institute for Plasma Research, Gandhinagar, India. The circular samples of W of the diameter of 10 mm and thicknesses of 1 mm to 3 mm were cut in four equal quadrants. The Gd samples were made from the GdO_2 powder (99.9 % pure). Pellets were made using pelletizer at the Physics Department, The M. S. University of Baroda, Vadodara. Gd samples were made in the pellet form with a radius of 0.65 cm and of thickness from 0.05 to 1.0 mm using Gd_2O_3 (99.9 %) powder. The weights of the samples were measured using digital weighing machine available at TIFR, Mumbai. The weights of W samples were 3.6689 g (Irradiation – 1), 0.7826 g (Irradiation – 2), 0.8344 g (Irradiation – 3) and 0.504 g (Irradiation – 4). The samples of Gd weighing 0.4071 g (irradiation – 1) and 0.9102 g (irradiation – 3) were used.

4.2.2 Neutron Irradiation at TIFR

The experiment was carried out using the 14UD BARC-TIFR Pelletron facility in Mumbai, India. A schematic layout of the Pelletron is given in FIG 4.1(a). The neutrons were produced using $^{7}Li(p, n)^{7}Be$ reaction. A proton beam was targeted on natural lithium foil of thickness 8.0 mg/cm^2 at 6.0 m from the analyzing magnet. The Li foil was wrapped with 3.7 mg/cm^2 tantalum in front and 4.12 mg/cm^2 in the back side like a sandwich structure. The samples were enclosed with aluminum foil to avoid contamination. The targets were irradiated with four different selected proton energies: 7.0, 11.0, 15.0 and 18.8 MeV. The spread of the proton energy at 6 m height was maximum 50 – 90 keV. The samples were kept at a distance of 2.1 cm from the Li - target in the forward direction. The targets were irradiated for different irradiation time. The irradiation details are given in Table 4.1. A schematic view of irradiation setup is shown in FIG 4.1(b). In each irradiation, the Indium (In) and thorium (Th) foils were used as flux monitor. After a suitable cooling time, the irradiated samples were mounted on different perspex plates and kept in front of the pre-calibrated High Purity Germanium (HPGe) detector. A Baltic company HPGe detector with 4k channels MCA and MAESTRO spectroscopic software were used to measure the

gamma ray spectra from the irradiated samples. The gamma spectrometer setup for activity counting is shown in FIG 4.1(c). The HPGe detector system was calibrated using standard ^{152}Eu multi-gamma source. The efficiency of the detector was also calculated at different energies using the same source. The gamma ray activities of the irradiated samples were measured for different counting time. The prominent gamma energies emitted from the irradiated samples and other spectroscopic data are given in Table 4.2. Isotopic abundances are taken from literature [14]. The threshold energies of the reactions are calculated using Q – value calculator provided online by NNDC [15]. The product half-life and details of the emitted prominent gamma rays are taken from ENDSF database [16]. Typical gamma ray spectra obtained from the irradiated W and Gd samples are shown in FIG 4.2 (a-b).

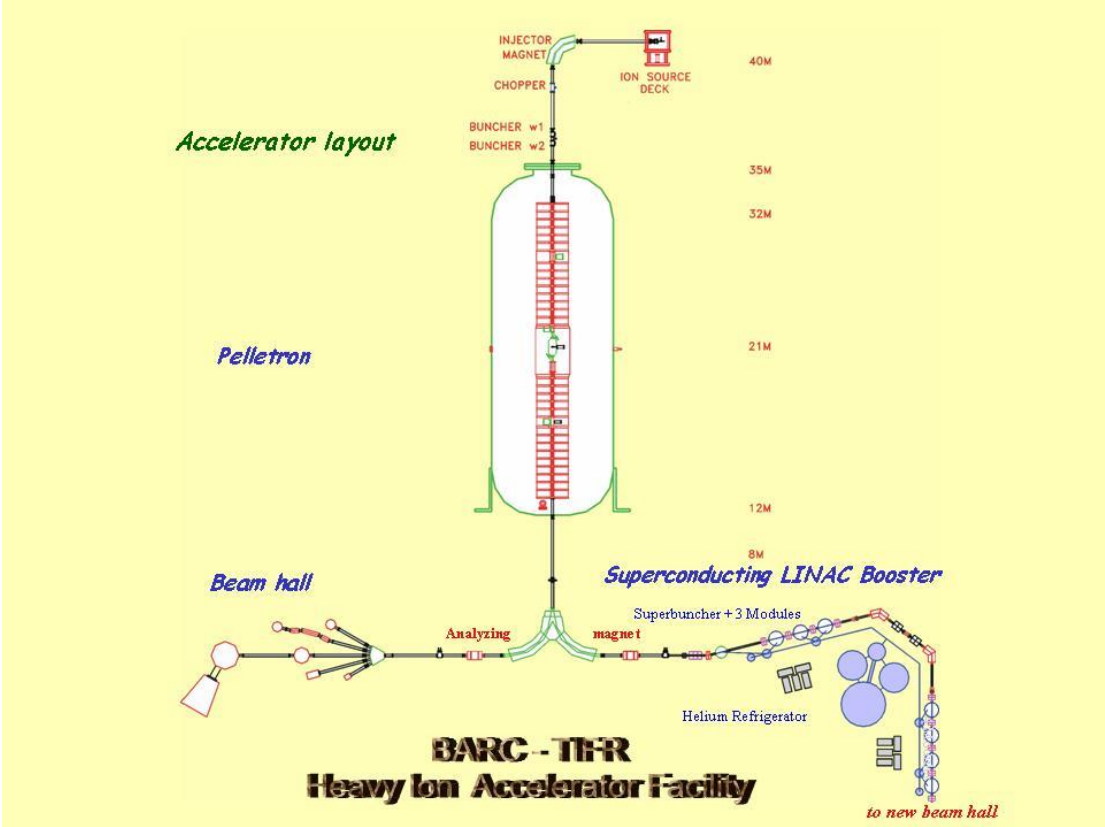

FIG 4.1(a) 14 UD TIFR-BARC Pelletron facillity

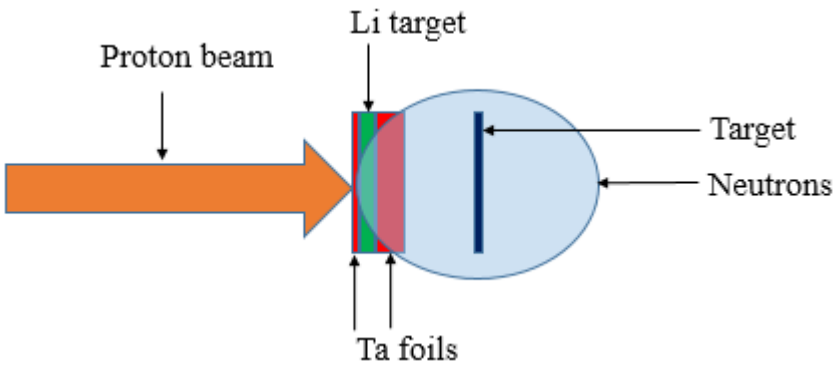

FIG 4.1(b) Experimental arrangement showing neutron production using Li (p, n) reaction

FIG 4.1(c) Gamma spectroscopy system for activity measurement

Table 4.1 Details of the irradiation at TIFR

	Irradiation - 1	**Irradiation-2**	**Irradiation-3**	**Irradiation-4**
Proton Energy (MeV)	18.8	7.0	15.0	11.0
Total Irradiation Time (hr:mm)	5:00	11:15	7:00	16:05
Beam Current (nA)	150	110	150	120

Table 4.2 Selected nuclear reactions, isotopic abundance, threshold energy of reaction, product isotope with half-life and prominent gamma ray energies with branching intensities

Reaction	**Isotopic Abundance (%) [14]**	**Threshold Energy (MeV) [15]**	**Product Nucleus**	**Half-life [16]**	**Prominent γ-ray (in keV) (Branching intensity %) [16]**
^{186}W(n, γ)^{187}W	28.43	-	^{187}W	24.0 h	479.5(26.6); 685.7(33.2)
^{182}W(n, p)^{182}Ta	26.50	1.037	^{182}Ta	114.74 d	1121.3(35.24)
^{154}Gd(n, 2n)^{153}Gd	2.18	8.953	^{153}Gd	240.4 d	103.1 (21.1)
^{160}Gd(n, 2n)^{159}Gd	21.86	7.498	^{159}Gd	18.479 h	363.5 (11.78)

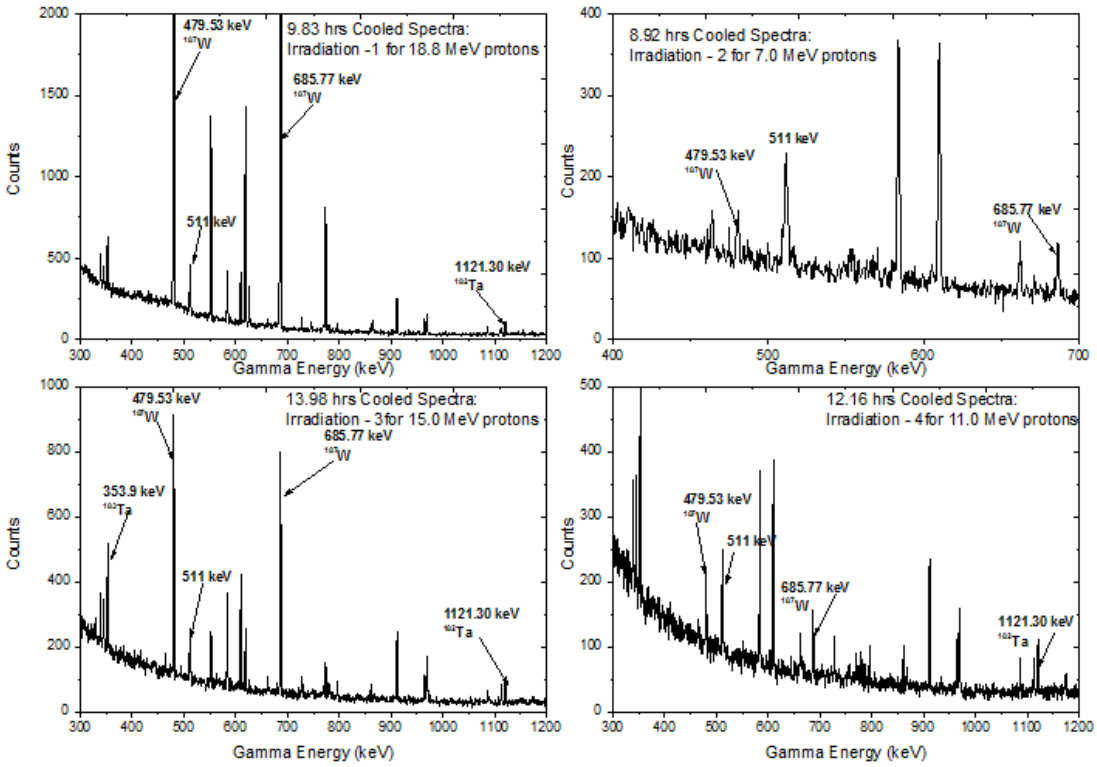

FIG 4.2(a) Typical γ-ray spectra for W targets obtained by using HPGe detector

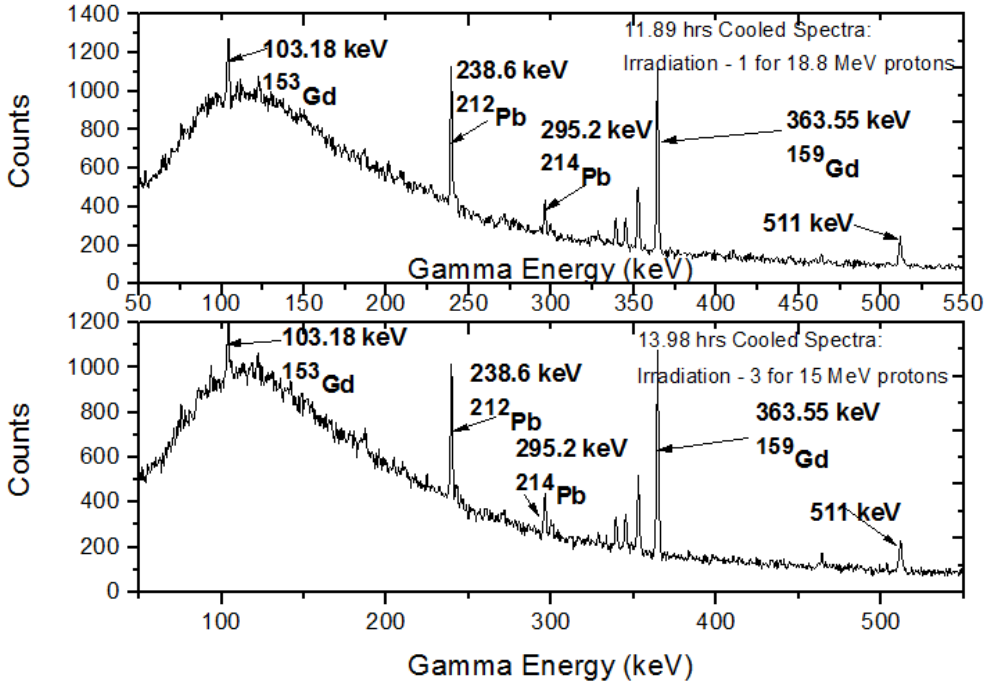

FIG 4.2(b) Typical γ-ray spectra for Gd targets obtained by using HPGe detector

4.3. Data analysis

4.3.1 Neutron Activation Analysis

The neutron activation analysis (NAA) method has already been discussed in Chapter – 1. The experimental data were analyzed by using this technique. A neutron interacts with the target nucleus and excites it by transferring the kinetic energy and it may follow the nuclear reaction. Through the nuclear reaction, the target nucleus transmutes into another product nucleus. This product nucleus may be radioactive and have certain half-life to decay. During the decay, it emits the radiation. This decay radiation carries the information of the production of the excited nucleus. The nuclear reaction rate or the rate of production of product isotopes depends on the number of target nuclei available and the neutron flux incident on it, as mentioned in eq. 1.13 of Chapter – 1. This method is usually used to measure reaction cross section by irradiating the target isotope with neutrons. The total production of the product nuclei can be measured by the characteristic gamma rays emitted from it. The cross section of the selected reactions can be determined using the following eq. 4.1 [17]. The derivation of eq. 4.1 is discussed in Chapter – 1.

$$\sigma = \frac{A_\gamma \cdot \lambda \cdot (t_c/t_r)}{N \cdot \emptyset \cdot I_\gamma \cdot \varepsilon \cdot (1-e^{-\lambda \cdot t_i}) \cdot (1-e^{-\lambda \cdot t_c}) \cdot e^{-\lambda \cdot t_w}} \qquad 4.1$$

Where,

A_γ= Number of detected gamma ray counts;

λ = Decay constant of product nucleus (s^{-1})

t_i = Irradiation time (s);

t_w = Cooling time (s);

t_c = Counting time (s);

t_r = Real time (Clock time) (s);

$\emptyset$ = Incident neutron flux ($n/cm^2/s$);

I_γ= Branching intensity of γ -ray;

ε = Efficiency of the detector for the chosen gamma ray;

N = Number of target atoms

In the above equation, the activity A_γ is measured using the HPGe detector for selected gamma rays emitted from the radioactive product isotope. The detector efficiency for different gamma ray energies was measured using ^{152}Eu multi-gamma

ray source. Keeping in view the half-lives of the interested isotopes, several rounds of gamma ray countings were done. The dead time of the detector system was kept below 0.6 % during the entire counting process. The numbers of target nuclei were calculated from the weight of the sample and isotopic abundances. The calculation of the neutron flux was done using the gamma ray spectra of irradiated In and Th foils. Other standard parameters of the reactions were taken from literature [14-16]. The cross section measurements of selected reactions along with other parameters are given in Table 4.2.

4.3.2 Peak average neutron energy

The neutrons were generated via ^{7}Li(p, n)^{7}Be reactions. The reaction Q – value is -1.886 MeV. Below 2.4 MeV, this reaction produces mono-energetic neutrons [18]. Above 2.4 MeV, the first excited state of ^{7}Be at 0.43 MeV may populate and produce the second group of neutrons [18, 19]. Above 6 MeV, the three body interaction takes place, and other excited states also get populated which can contribute to neutron production along with the main neutron group [18, 19]. Hence the source is not a pure mono energetic source. Although there are lower energy sub-group of neutrons, the primary (main) group of neutrons have always larger flux and can be used to measure the reaction cross section. The spectrum averaged neutron energy can be calculated using eq. 4.2 [20]. In this equation, one has to calculate the convolution of neutron flux values and energies, which are forming the peak neutrons. This is given by the numerator term in eq. 4.2. The denominator term gives the total neutron flux under the peak. The ratio of these two terms gives the spectrum peak averaged neutron energy. The neutron spectra corresponding to all the four incident proton energies are shown in FIG 4.3(a). And the FWHM energy has been taken for this energy range. This can be visualized in FIG 4.3(b). To calculate the neutron peak average energy, one has to take the energies from the starting energy of peak forming (E_{ps}) to peak ending (maximum, E_{max}) neutron energy and respective neutron production cross section/flux ($\emptyset_i$) with possible energy bins. The integration of the multiplications of E_i and $\emptyset_i$ taken between this two mention energy limits. Then it is divided with the total $\emptyset_i$ in between this energies.

$$E_{mean} = \frac{\int_{Eps}^{Emax} E_i \emptyset_i dE}{\int_{Eps}^{Emax} \emptyset_i dE} \quad 4.2$$

where E_{ps} = peak neutron energy forming start energy of the reaction

E_{max} = maximum neutron energy

E_i = energy bin

$\emptyset_i$ = neutron flux of energy bin E_i

E_{mean} = effective mean energy

The neutron spectra for 7.0, 11.0, 15.0 and 18.8 MeV proton energies were derived by taking data from various available literature [18-22].

4.3.3 Neutron Flux Calculation

In order to analyze the data, it is necessary to accurately calculate the neutron flux incident on the target. In the present experiment, ^{115}In(n, n′)^{115m}In and ^{232}Th(n, f)^{97}Zr were taken as monitor reactions for neutron flux measurement. The product nuclei of the reaction products ^{115m}In and ^{97}Zr have half-lives of 4.486 h and 16.749 h respectively [16]. The emitted characteristic gamma lines are given in Table 4.4. Typical gamma ray spectra obtained from both the monitors are shown in FIG 4.4.

The calculations of neutron flux incident on the target were done by using the spectrum averaged neutron cross section for the above monitor reactions by using the data available EXFOR data library [1]. The spectrum average cross section was calculated using the following eq. 4.3.

$$\sigma_{av} = \frac{\int_{Eth}^{Emax} \sigma_i \emptyset_i dE}{\int_{Eth}^{Emax} \emptyset_i dE} \quad 4.3$$

where E_{th} = threshold energy of the monitor reaction

E_{max} = maximum neutron energy

σ_i = Cross section at energy E_i for monitor reaction from EXFOR [23-30]

$\emptyset_i$ = neutron flux of energy bin E_i from the FIG 4.3 (a – c)

σ_{av}= Spectrum averaged cross section

The neutron flux incident on targets for all the four irradiations was calculated using the following activation, which is derived from eq. 4.1.

$$\emptyset = \frac{A_\gamma \cdot \lambda \cdot (t_c/t_r)}{N \cdot \sigma_{av} \cdot I_\gamma \cdot \varepsilon \cdot (1-e^{-\lambda \cdot t_i}) \cdot (1-e^{-\lambda \cdot t_c}) \cdot e^{-\lambda \cdot t_w}} \quad 4.4$$

All the parameters are similar to eq. 4.1.

In the case of fission reaction monitor, the fission yield term (Y) will come in the denominator on the right side of the above eq. 4.4. In the cross section calculations, the measured values of the average neutron flux from both the monitors were taken, as both, these values are in agreement with each other within the limits of the experimental error.

4.4. Cross section correction for lower energy neutrons

In order to measure the cross section accurately, it is necessary to make corrections due to the contributions from lower energy neutrons. This correction is not required when the neutron source is purely mono-energetic, which is not in the present case. As mentioned earlier, in addition to a primary neutron group, there exist secondary neutron groups. The contributions from secondary neutrons are due to the excited state of ^{7}Be and three-body reactions above 2.4 and 6 MeV respectively [18]. These secondary groups produce neutrons at energy lower in addition to the primary group neutrons [18, 19]. As the primary neutrons peak is always at much higher energy, it can be considered as a quasi mono-energetic source. It is possible to remove the contributions of low energy neutrons from the primary neutron groups by the process of tailing correction. In the present measurement, the tailing correction has been done using the method given in the literature [20].

First, the cross sections have been calculated using the NAA eq. 4.1 and neutron flux from monitor reactions. For a capture reaction, one has to use total neutron flux, but for the reactions having threshold energy, the neutron flux must be corrected i.e. the neutrons from threshold to maximum energy neutrons. To do this, one has to remove the neutron flux from minimum to threshold energy neutrons, by taking the area under the neutron spectra. For instance, ^{154}Gd(n, 2n)^{153}Gd reaction has threshold energy of 8.953 MeV. Hence, the flux for this reaction must be the area under the curve shown

from '**A'** (threshold energy) to '**B'** (maximum neutron energy) as shown in FIG 4.3(c). This will correct the actual neutron flux, which has produced the desired product isotopes. Using the correct neutron flux, a set of cross sections for all reactions has been calculated. These cross sections are from all the neutron flux including the peak area neutrons. In order to remove the effective spectrum average cross section from threshold to the energy from which peak is starting forming (E_{ps}), it is necessary to take the help of theoretical calculations using modular code TALYS – 1.8 or data available in different evaluated data libraries, to obtain the reaction cross section. These calculated cross sections at different energies are convoluted with the neutron flux. The spectrum average cross section for each reaction was calculated from threshold to energy E_{ps}, and it is subtracted from the previous cross section dataset. The final value thus obtained gives the cross section for the reaction at the spectrum average neutron peak energy.

Using the above method, the cross section for the $^{182}W(n, p)^{182}Ta$, $^{186}W(n, \gamma)^{187}W$, $^{154}Gd(n, 2n)^{153}Gd$ and $^{160}Gd(n, 2n)^{159}Gd$ reactions were measured at the neutron energies of 5.08, 8.96, 12.47 and 16.63 MeV. In the ^{160}Gd (n, 2n) ^{159}Gd and ^{158}Gd (n,γ) ^{159}Gd reactions, a common γ-ray of 363.55 keV (I_γ=11%) is emitted. Therefore, it is necessary to remove the part of the cross section from this capture reaction. At higher energy, the (n, γ) reaction has very small contribution as compared to the lower energy neutrons. Since the lower energy neutron part has been already corrected using the above method, therefore the cross section obtained is purely due to the (n, 2n) reaction. In the same way, the tailing corrections have been applied for all the reactions studied in the present work. The major uncertainties in the measured cross sections are given in Table 4.5.

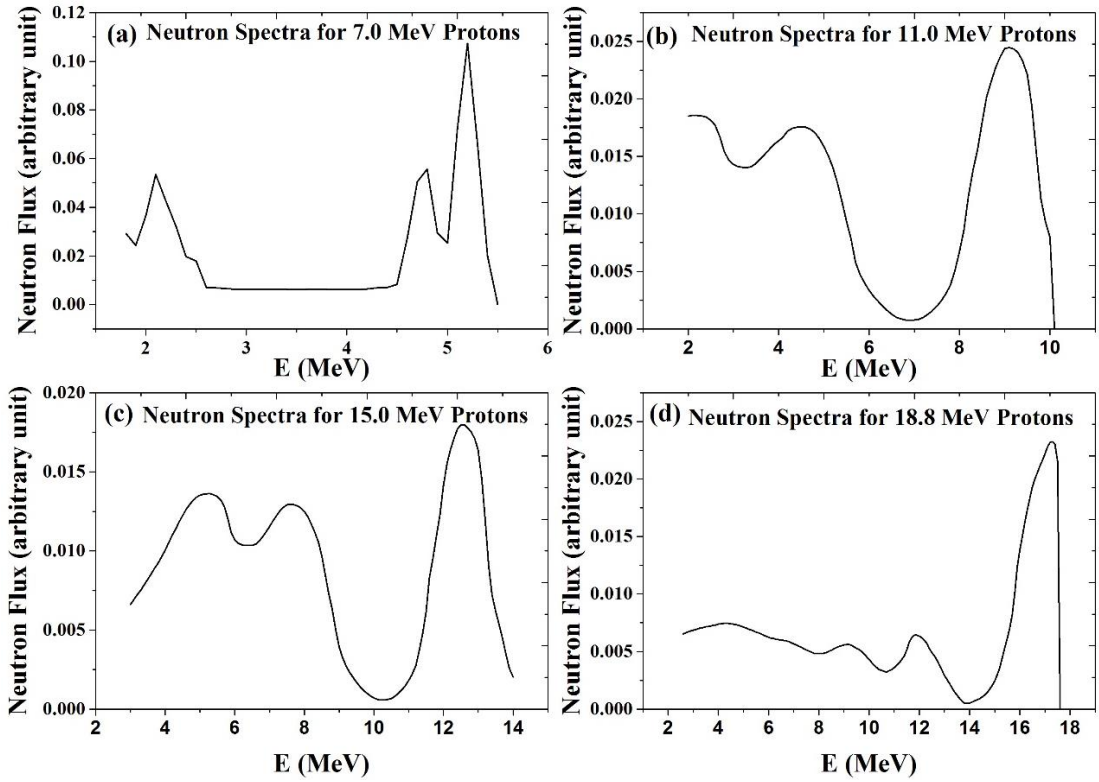

FIG 4.3(a) ^{7}Li (p, n) ^{7}Be neutron spectra for the 7.0, 11.0, 15.0 and 18.8 MeV proton energies

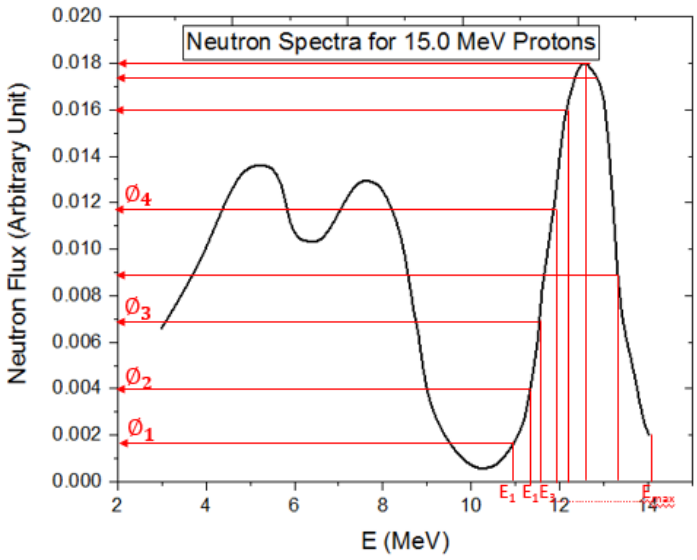

FIG 4.3(b) Visualization of peak averaged neutron energy for 15 MeV neutron peak

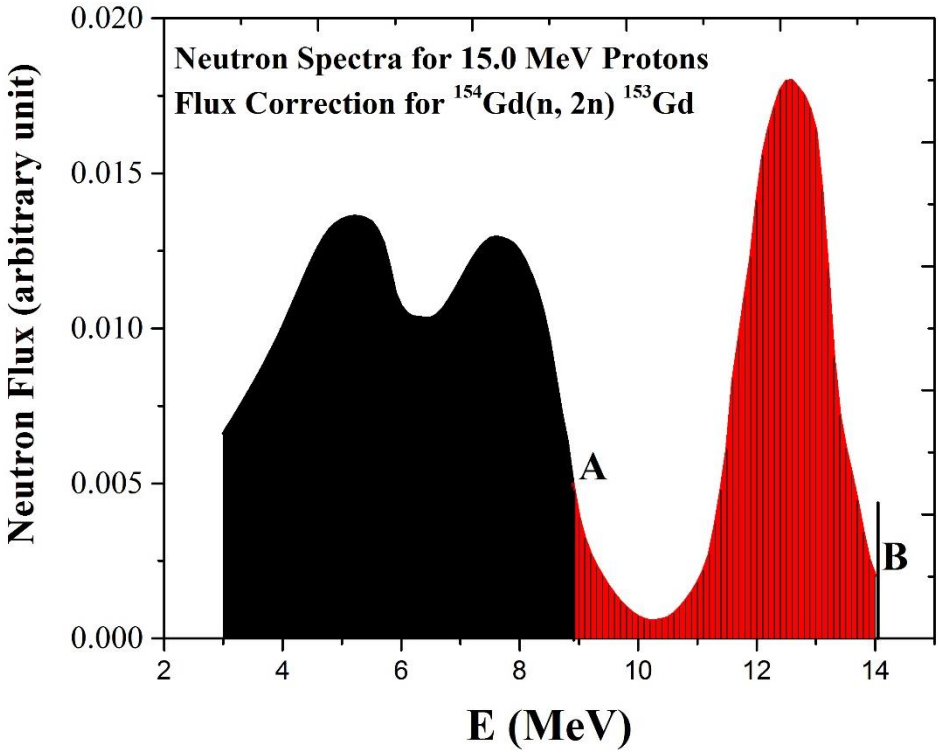

FIG 4.3(c) Neutron flux correction for the threshold energy reactions, shown for ^{154}Gd (n, 2n) ^{153}Gd reaction with threshold energy of 8.953 MeV labeled by **'A'** and maximum neutron energy labeled by **'B'**

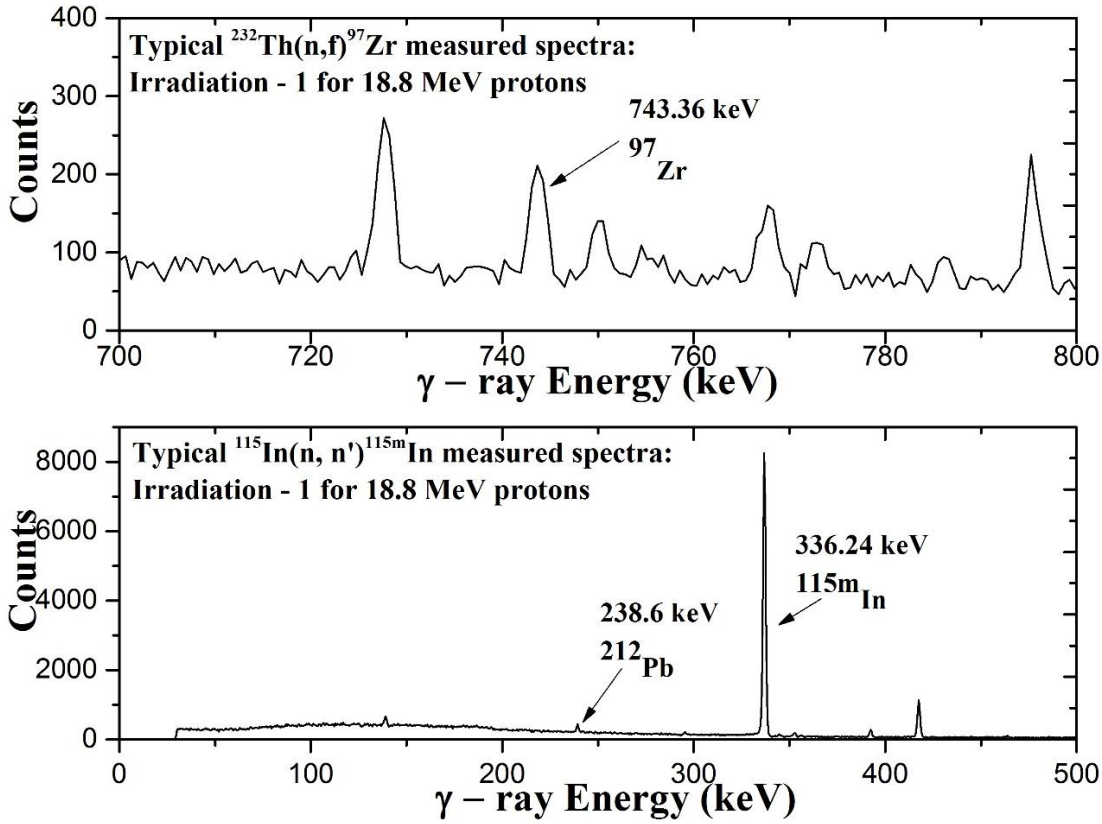

FIG 4.4 Typical monitor reaction gamma ray spectra using HPGe detector

Table 4.3 The spectrum averaged neutron energies and respective neutron flux from two different monitor reactions

	Irradiation - 1	**Irradiation-2**	**Irradiation-3**	**Irradiation-4**
Proton Energy (MeV)	18.8	7.0	15.0	11.0
Neutron Energy from eq. (2) (MeV)	16.63 ± 0.95	5.08 ± 0.165	12.47 ± 0.825	8.96 ± 0.77
Spectrum Averaged Cross section for In monitor (mb)	188.94	223.88	253.79	302.85
Calculated Neutron Flux from ^{115}In(n, n')^{115m}In (n cm^{-2} s^{-1})	6.2891×10^7	4.6304×10^6	1.8054×10^7	1.6009×10^6
Spectrum Averaged Cross section for Th monitor (mb)	341.67	99.04	269.58	220.01
Calculated Neutron Flux from ^{232}Th(n, f)^{97}Zr (n cm^{-2} s^{-1})	6.2885×10^7	4.5709×10^6	1.7090×10^7	1.5850×10^6

Table 4.4 The monitor reaction with the product isotope and prominent gamma lines

Monitor Reaction	**Product Nucleus (Half-life)** [16]	**Prominent gamma Line (in keV) (branching Intensity %)** [16]
^{115}In(n, n')^{115m}In	^{115m}In (4.486 h)	336.24 (45.8)
^{232}Th(n, f)^{97}Zr	^{97}Zr (16.749 h)	743.36 (93.0)

4.5. Theoretical calculations

In order to theoretically understand the measured cross section results, two well-known nuclear reactions modular codes TALYS – 1.8 and EMPIRE – 3.2.2 were used [13]. Both the codes are being used worldwide for nuclear data prediction for the emission of gamma, neutron, proton, deuteron, triton and other particles. Both codes used the reaction parameters from the RIPL database [31]. These codes consider the effect of level density parameters, compound, pre-equilibrium and direct reaction mechanism as a function of incident particle energy. The optical model parameters were obtained by using a global potential, proposed by Koning and Delaroche [32]. The compound reaction mechanism was incorporated using the Hauser-Feshbach model [33]. The pre-equilibrium contribution was accounted by an exciton model that was developed by Kalbach [34]. In the present work, the calculations have been done with all the default parameters except changing the ldmodel and level density parameters. The present results along with EXFOR data were compared with these predicted data as shown in FIG 4.5 (a-d).

4.6. Results and discussion

The main objective of the present study was to provide a set of reaction cross section data in the energy range where there are very few or no measurements available in the literature. These cross sections are important for the accurate reactor design and also to improve the existing nuclear database. Hence the present experimental data for W and Gd isotopes become more important. Further, in this energy region, the standard nuclear models play an important role to validate the present measured experimental data. The major uncertainties in the present reaction cross sections are given in Table 4.5.

The measured data were supported by the theoretical predictions using EMPIRE – 3.2.2 and TALYS – 1.8. There are different options of level density given in EMPIRE – 3.2.2. The level density parameter value levden = 0, 1, 2, 3, 4 uses various well known models described in various publications [31, 35-39]. By varying these parameters, the cross sections for the selected reactions from threshold to 20 MeV were calculated. The predicted and experimental results are shown in FIG 4.5 (a-d). In TALYS – 1.8, the different ldmodel options were varied from ldmodel1 to ldmodel6

for the selected nuclear reactions and the experimental cross sections were compared. The details of these parameters are given in the TALYS – 1.8 manual [39, 40].

As shown in FIG 4.5 (a) for $^{186}W(n, \gamma)^{187}W$ reaction, the levden = 2 of EMPIRE – 3.2.2 gives a relatively better agreement compared to other levden values. But at the lower energy, the levden = 2 does not give satisfactory predictions. Moreover, all other level density models of EMPIRE – 3.2.2 show discrepancies with each other and predicts lower cross section as compared to the present experimental results. In the case of TALYS – 1.8 analyses, results of all the ldmodels options are in good agreement with the data of present measurements. For the ^{182}W (n, p) ^{182}Ta reaction, all TALYS – 1.8 ldmodels are in good agreement. The EMPIRE levden models show a discrepancy with most of the EXFOR and the present data. For the ^{154}Gd (n, 2n) ^{153}Gd and ^{160}Gd (n, 2n) ^{159}Gd reactions, the experimental results are in good agreement with both the TALYS – 1.8 and EMPIRE – 3.2.2 predictions, except levden = 2, being listed as a future option in the EMPIRE input file. Only the measurement at 16.63 MeV neutron energy of $^{160}Gd(n, 2n)^{159}Gd$ is underestimated than the predicted values. Overall the theoretical predictions support the present results. The measured cross section values and the different model predicted values are compared at the same energies in Table 4.6. In general, TALYS – 1.8, for all the selected models, gives better agreement compared to EMPIRE – 3.2.2 in predicting the present experimental results.

Table 4.5 Major uncertainties incorporated in the present cross section results

Parameter	**Limit (%)**
Counting rate	≤ 4 - 5
Efficiency Calibration	≤ 3
Self - absorption	≤ 0.2
Mass	≤ 0.001
Neutron flux	≤ 6
I_γ	≤ 3

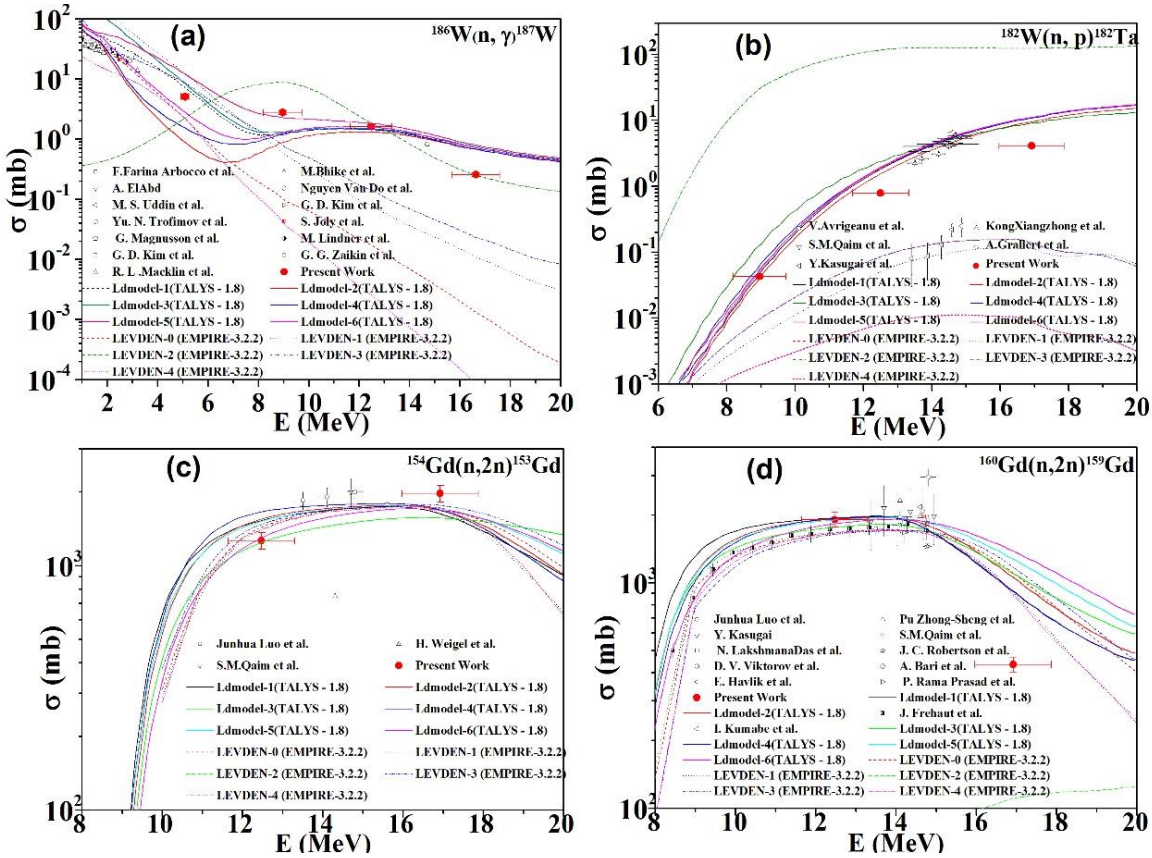

FIG 4.5 Present measured cross section for $^{186}W(n, \gamma)^{187}W$ and $^{182}W(n, p)^{182}Ta$, $^{154}Gd(n, 2n)^{153}Gd$ and $^{160}Gd(n, 2n)^{159}Gd$ reactions compared with EXFOR and predicted cross section data using different theoretical nuclear models of TALYS – 1.8 and EMPIRE – 3.2.2; The LEVDE-2 model of EMPIRE – 3.2.2 predicts very low values (below 100 mb) of cross sections comparing to other models hence it cannot be seen in plot of $^{154}Gd(n, 2n)^{153}Gd$

4.7. Summary and conclusions

Cross section for the $^{182}W(n, p)^{182}Ta$, $^{186}W(n, \gamma)^{187}W$, $^{154}Gd(n, 2n)^{153}Gd$ and $^{160}Gd(n, 2n)^{159}Gd$ reactions were measured at the neutron energies 5.08 ± 0.165, 8.96 ± 0.77, 12.47 ± 0.825 and 16.63 ± 0.95 MeV by using the neutron activation analysis technique and incorporating standard tailing corrections [18]. The cross sections have been measured in an energy range where very few or no measurements are available. The different correction terms are discussed in order to achieve accurate cross section results. The spectrum averaged neutron energy and accurate flux measurements have also been duly incorporated. The neutron flux at different energies have been calculated by using two monitor reactions and the values thus obtained were found to be in good agreement. The average flux values from the two monitor reactions were taken for cross sections calculation. The cross section for the $^{186}W(n, \gamma)^{187}W$ reaction have been measured at four different energies. In the case of $^{182}W(n, p)^{182}Ta$ the cross sections are reported at 8.96 ± 0.77, 12.47 ± 0.825 and 16.63 ± 0.95 MeV. For the $^{154}Gd(n, 2n)^{153}Gd$ and $^{160}Gd(n, 2n)^{59}Gd$ reactions, the cross sections are reported at 12.47 ± 0.825 and 16.63 ± 0.95 MeV neutron energies. All the measurements have been compared with the theoretical modular codes TALYS – 1.8 and EMPIRE – 3.2.2. It may be concluded that TALYS – 1.8 gives an overall satisfactory agreement with the present experimental and EXFOR results for most of the selected ldmodels as compared to EMPIRE – 3.2.2 predictions. However, in the case of (n, γ) reaction, levden = 2 of EMPIRE gives somewhat better predictions as compared to other levden models in the energy region above 12 MeV. The cross section data presented in this work are important for the future fission/fusion reactor technology.

References

[1] A. J. Koning, and J. Blomgren, Nuclear data for sustainable nuclear energy, JRC Scientific and Tech. Rep. EUR23977EN-2009, 15 (2009).

[2] Cross Section Information Storage and Retrieval System (EXFOR), IAEA, Vienna, Austria. http://www.nds.iaea.or.at/exfor/ (online).

[3] M. Lehnen, *et al*., J. Nucl. Mater. **463**, 39 (2013).

[4] J. Qing, Y. Wu, M. Regis, and J. W. Kwan, IEEE Trans. Nucl. Sci. **56**, 1312 (2009).

[5] J. Reijonen, F. Gicquel, S. K. Hahto, M. King, T. P. Lou, and K. N. Leung, Appl. Radiat. Isotopes **63**, 757 (2005).

[6] Y. Wu, J. P. Hurley, Q. Ji, J. Kwan, and K. N. Leung, IEEE Trans. Nucl. Sci. **56**, 1306 (2009).

[7] V. Voitsenya, *et al*., Rev. Sci. Instrum. **72**, 475 (2001).

[8] G. De Temmerman, R. A. Pitts, V. S. Voitsenya, L. Marot, G. Veres, M. Maurer, and P. Oelhafen, J. Nucl. Mater. **363**, 259 (2007).

[9] K. H. Behringer, J. Nucl. Mater.**145**, 145 (1987).

[10] Yousry Gohar, Igor Bolshinsky, and Ivan Karnaukhov, NEA/NSC/DOC (2015) 7, 254 (2015).

[11] R. Vijayalakshmi, D. K. Singh, M. K. Kotekar, and H. Singh, J Radioanal. Nucl. Chem. **300**, 129 (2014)

[12] S. Dutta, P. Suryanarayanan, A. R. Kandalgaonkar, R. S. Sharma, and H. Bose, BARC News Lett, **271**, 2 (2006).

[13] N. Dzysiuk, I. Kadenko, A. J. Koning, and R. Yermolenko, Phys. Rev. C **81**, 014610 (2010).

[14] K. J. R. Rosman, and P. D. P. Taylor, Pure Appl. Chem. **71**, 1593 (1999).

[15] http://www.nndc.bnl.gov/qcalc/index.jsp, retrieved on 11th November 2016.

[16] http://www.nndc.bnl.gov/nudat2/indx_dec.jsp, retrieved on 21st March 2017.

[17] Vibha Vansola, *et al*., Radiochim. Acta **103**, 817 (2015).

[18] C. H. Poppe, J. D. Anderson, J. C. Davis, S. M. Grimes, and C. Wong, Phys. Rev. C **14**, 438 (1976).

[19] J. D. Anderson, C. Wong, and V. A. Madsen, Phys. Rev. Letts. **24**, 1074 (1970).

[20] D. L. Smith, *et al*., " Corrections for Low Energy Neutrons by Spectral Indexing", Retrieved from: https://www.oecdnea.org/science/docs/2005/nsc-wpec-doc2005-357.pdf

[21] P. M. Prajapati, *et al*., Eur. Phys. J. A **48**, 1 (2012).

[22] M. W. Mcnaughton, N. S. P. King, F. P. Brady, J. L. Romero, and T. S. Subramanian, Nucl. Instrum. Methods 130, 555 (1975).

[23] A. A. Lapenas, Neutron Spect. Meas. by Activ., Riga 1975, (1975).

[24] G. Loevestam, M. Hult, A. Fessler,T. Gamboni, J. Gasparro, R. Jaime, P. Lindahl, S. Oberstedt, and H. Tagziria, Nucl. Instrum. Methods in Physics Res., Sect. A 580, 1400 (2007).

[25] Y. Agus, I. Celenk, and A.Ozmen Radiochimica Acta 92, 63 (2004).

[26] M. S. Uddin, Radiochimica Acta 101, 613 (2013).

[27] O. A. Shcherbakov, *et al*., Int. Sem. on Interactions of Neutrons with Nuclei 9, 257 (2001).

[28] R. K. Jain, Pramana 49, 515 (1997).

[29] I. Garlea, Chr.Miron-Garlea, and H. N. Rosu, Revue Roumaine de Physique 37, 19 (1992).

[30] F. Manabe, K. Kanda, T. Iwasaki, H. Terayama, Y. Karino, M. Baba, and N. Hirakawa, Fac. of Engineering, Tohoku Univ. Tech. Report 52, 97 (1988).

[31] R. Capote, et al., Nuclear Data Sheets 110, 3107 (2009).

[32] A. J. Koning, and J. P. Declaroche, Nucl. Phys. A 713, 231(2003).

[33] W. Hauser, and H. Feshbach, Phys. Rev. 87, 366 (1952).

[34] C. Kalbach, Phys. Rev. C **33**, 818 (1986).

[35] https://www-nds.iaea.org/RIPL-3/densities/, retrieved on 28th February 2017.

[36] A. V. Ignatyuk, K. K. Istekov, and G. N. Smirenkin, Sov. J. Nucl. Phys. **29**, 450 (1979).

[37] A.V. Ignatyuk, J. L. Weil, S. Raman, and S. Kahane, Phys. Rev. C **47**, 1504 (1993).

[38] A. Gilbert, and A. G. W. Cameron, Can. J. Phys. **43**, 1446 (1965).

[39] S. Hilaire, M. Girod, S. Goriely and A. J. Koning, Phys. Rev. C **86**, 1 (2012).

[40] A. Koning, S. Hilaire, and S. Goriely, TALYS-1.6 - A Nuclear Reaction Program, User Manual, 1stedition (NRG, The Netherlands, 2013).

Table 4.6 Comparison of present experimental data different model predictions using TALYS – 1.8 and EMPIRE – 3.2.2

Energy (MeV)	$^{186}W(n, \gamma)^{187}W$ reaction cross section (mb)											
	Measured	TALYS - 1.8						EMPIRE – 3.2.2				
		Ldmodel-1	Ldmodel-2	Ldmodel-3	Ldmodel-4	Ldmodel-5	Ldmodel-6	Levden-0	Levden-1	Levden-2	Levden-3	Levden-4
5.08±0.165	5.079±0.39	7.23	0.885	8.37	1.53	12.1	2.80	2.24	12.8	2.24	8.83	2.2903
8.96±0.77	2.767±0.19	1.22	0.871	1.31	1.17	2.26	1.26	0.108	0.618	9.01	0.827	0.0453
12.47±0.825	1.620±0.11	1.46	1.30	1.48	1.43	1.81	1.58	0.0181	0.0794	1.86	0.146	0.0027
16.63±0.95	0.257±0.02	0.726	0.676	0.753	0.683	0.799	0.716	0.00129	0.0107	0.249	0.0226	8.41E-5
Energy (MeV)	$^{182}W(n, p)^{182}Ta$ reaction cross section (mb)											
	Measured	TALYS - 1.8						EMPIRE – 3.2.2				
		Ldmodel-1	Ldmodel-2	Ldmodel-3	Ldmodel-4	Ldmodel-5	Ldmodel-6	Levden-0	Levden-1	Levden-2	Levden-3	Levden-4
8.96± 0.77	0.043±0.003	0.04813	0.04141	0.12659	0.06359	0.05509	0.05307	0.00964	0.00544	31.0747	0.00964	0.00194
12.47±0.825	0.793±0.06	1.789	1.52	2.33301	1.87	1.86	1.92	0.0842	0.0495	118	0.0842	0.00803
16.63±0.95	4.092±0.28	10.2	8.89	8.4404	10.2	10.4	10.5	0.163	0.147	124	0.163	0.0107
Energy (MeV)	$^{154}Gd(n, 2n)^{153}Gd$ Cross Section (mb)											
	Measured	TALYS - 1.8						EMPIRE – 3.2.2				
		Ldmodel-1	Ldmodel-2	Ldmodel-3	Ldmodel-4	Ldmodel-5	Ldmodel-6	Levden-0	Levden-1	Levden-2	Levden-3	Levden-4
12.47±0.825	1265 ±98	1534	1556	1248	1659	1520	1298	1444	1412	22.2	1479	1397
16.63±0.95	1973±153	1683	1725	1571	1737	1735	1703	1748	1744	65.3	1774	1744
Energy (MeV)	$^{160}Gd(n, 2n)^{159}Gd$ Cross Section (mb)											
	Measured	TALYS - 1.8						EMPIRE – 3.2.2				
		Ldmodel-1	Ldmodel-2	Ldmodel-3	Ldmodel-4	Ldmodel-5	Ldmodel-6	Levden-0	Levden-1	Levden-2	Levden-3	Levden-4
12.47±0.825	1913±143	1938	1919	1765	1935	1901	1828	1669	1679	52.9	1642	1660
16.63±0.95	435±33	1009	1155	1183	1005	1364	1465	1213	1027	106	1282	999